Accepted Manuscript

Use of light for the electrochemical deposition of Bi on n-GaAs substrates

Alicia Prados, Rocío Ranchal

PII:	S0013-4686(19)31018-7
DOI:	10.1016/j.electacta.2019.05.085
Reference:	EA 34226
To appear in:	*Electrochimica Acta*
Received Date:	25 February 2019
Accepted Date:	16 May 2019

Please cite this article as: Alicia Prados, Rocío Ranchal, Use of light for the electrochemical deposition of Bi on n-GaAs substrates, *Electrochimica Acta* (2019), doi: 10.1016/j.electacta.2019.05.085

Use of light for the electrochemical deposition of Bi on n-GaAs substrates

Alicia Prados and Rocío Ranchal

Dpto. Física de Materiales, Universidad Complutense de Madrid. Ciudad Universitaria s/n, Madrid 28040, Spain

*Corresponding author: a.prados@ucm.es Phone: (+34) 91 394 5012;

Fax: (+34) 91 394 4547

Abstract

In this work, we have explored the possibility of using light to remove the adsorbed hydrogen layer that blocks the GaAs substrate surface when electrodepositing Bi thin films on lower-doped n-GaAs(111)B substrates. A light pulse of a few seconds applied under open-circuit (zero-current) conditions before starting the Bi electrodeposition in darkness has a small effect on the structural, morphological and interfacial electrical properties of the Bi film in comparison to layers deposited without the use of light. The potentiostatic curves recorded during the Bi nucleation show that the light pulse does not remove the adsorbed hydrogen layer but modifies the n-GaAs surface, inhibiting the reduction of Bi(III) ions. The atomic force microscopy analysis of the n-GaAs surface corroborates that the light degrades the surface by inducing photo-oxidation reactions, phenomenon that is correlated to the photocorrosion of the substrate. To maintain the electrical neutrality during photocorrosion, proton reduction and electroless deposition of Bi occur in parallel to the photo-oxidations. The simultaneity of these processes and the inhibition of Bi(III) ions to get reduced on those areas of the n-GaAs surface chemically altered enables the electroless deposition of unconnected Bi flakes with morphological, structural and interfacial electrical properties close to the state of the art of Bi thin films. Only the out of plane crystal quality of the Bi flakes show a small detriment whereas the Schottky barrier height slightly increases.

Keywords

Bismuth; n-GaAs; Nucleation; Electroless; Thermionic Emission.

1. Introduction

Bismuth (Bi) is a semimetal with interesting electronic properties due to the large carrier mean free path [1, 2] and Fermi wavelength. [3, 4]. Bi surface states are strongly spin-polarized via Rashba effect [5]. This makes Bi interesting for spintronics [6] as demonstrated by the large spin to charge conversion induced by spin-orbit coupling observed in the Bi/Ag interface. [7] In order to investigate the possibility of implementing Bi in spintronics devices, it is necessary to focus on the growth and characterization of Bi thin films since they represent a better configuration than other nanostructures to do so.

Compared to other growth techniques, electrodeposition offers a large number of advantages to grow Bi thin films since it provides high quality Bi on different substrates ([8] and references therein) at a high deposition rate, with a set-up transferable to industry and compatible with patterning. Among the possible substrates that can be used, semiconductors like GaAs can be very versatile in the development of Bi-based devices for several reasons. Rectifying [9] or tunnel [10, 11] Schottky barriers can be fabricated by varying the substrate doping level, obtaining different mechanisms for electron transport through the interface, thermionic emission or thermionic-field emission. Modifying the substrate surface orientation gives the opportunity to synthesize Bi thin films with both different crystalline textures and interfacial electrical properties. [10] Finally, the electrodeposition conditions have a strong impact not only on the morphological and crystal quality of the film but also on the electrical properties of the interface. [11, 12] However, one of the main drawbacks of electrodepositing Bi onto n-GaAs is the presence of an adsorbed hydrogen (H_{ads}) layer at the substrate surface that results from the interaction between the n-GaAs surface states and the protons of the electrolyte. [13] Although it might protect the n-GaAs surface form oxidation, it also hinders the nucleation of Bi(III) ions avoiding the growth of compact and high quality Bi thin films. To solve this problem, we designed a protocol to desorb the H_{ads} layer before carrying out the

Bi electrodeposition, so high-quality Bi layers can eventually be obtained. [14, 11, 10] Nevertheless, this protocol can only be used with highly-doped semiconducting substrates with a carrier concentration higher than $1 \cdot 10^{17}$ cm^{-3}, because it involves the dissolution of a previously deposited Bi layer. For n-GaAs substrates with a lower carrier concentration, that we will call from now on "lower-doped n-GaAs", we investigated another routine based on electrodepositing under illumination conditions [14] since the photogenerated holes can remove the H_{ads} layer. [15] However, this protocol leads to a rough and chemically modified interface because of the photocorrosion of the n-GaAs substrate upon illumination [16, 17, 18].

In this work, we have explored an alternative to this routine based on applying a light pulse of a few seconds under open-circuit (zero-current) conditions before electrodepositing Bi under darkness conditions on lower-doped n-GaAs(111)B substrates. The analysis of current density transients and atomic force microscopy (AFM) images indicates that the light pulse does not desorb the H_{ads} layer but produces the degradation of the n-GaAs substrate surface due to photo-oxidations. To maintain the electrical neutrality of the cell during the illumination under open-circuit conditions, parallel reduction reactions are necessary. In this case, these are protons and Bi(III) ion reduction, that seem to be inhibited on the areas that have been chemically altered by the photo-oxidations. We have taken these results into account to propose a new route for synthesizing unconnected Bi flakes by means of electroless deposition under continuous illumination at open-circuit conditions, which represents a step forward on the development of Bi-based nanodevices. Although electroless deposits can present different properties from their electrodeposited equivalents [19], we have observed pretty similar characteristics, except for slightly differences in the out-of-plane quality and the Schottky barrier height, for the Bi flakes.

2. Experimental

Electrochemical experiments have been carried out using a stable water-based electrolyte containing 1 mM Bi_2O_3 (bismuth oxide) as the Bi(III) cation source and 1 M $HClO_4$ (perchloric acid) as supporting electrolyte. Solutions were prepared with analytical grade chemicals and deionized water in order to avoid free ions. The pH of the solution (approximately 0.1) was not necessary to be further adjusted. Working electrodes were Si doped n-type GaAs(111)B wafers, supplied by Semiconductor Wafer Inc., with a carrier concentration of $n_0 = 4 \times 10^{16}$ cm^{-3}. Ohmic contacts were made on the back of the wafers by thermal evaporation of 80 nm of AuGe (2% Ge) and 250 nm of Au, followed by an annealing at 380 ^oC in forming gas for 90 s. The total surface area exposed to the electrolyte was 0.15 cm^2 in all cases. Prior to each experiment, substrates were degreased and then etched to remove GaAs native oxide under darkness conditions. First, substrates are dipped in a solution of HCl (10% vol.) for 2 min to remove arsenic and gallium oxides. [20] Then, substrates are rinsed in deionized water for 2 min to remove Ga-Cl_x species since they are soluble in water. [21] Finally, substrates are immersed in 1 M $HClO_4$ (supporting electrolyte) for 2 min to remove possible Cl^- ions remaining in the solution or adsorbed at the substrate surface. Then, the substrate surface is protected from air with a drop of 1M $HClO_4$ (supporting electrolyte) when transferred to the Bi(III) solution, where substrates remained 2 min to reach a stable open-circuit potential (OCP). In this condition, the substrate surface is oxide-free with about one monolayer coverage of elementary As, which interacts with the protons in the solution (As-H) [22], creating a layer of adsorbed hydrogen [13]. Electrochemical experiments were controlled by a PalmSens EmStat3+Blue potentiostat and carried out in a three-electrode cell with a platinum mesh as counter electrode and a Ag/AgCl (3 M NaCl) reference electrode supplied by BASi (E_{eq} = 0.196 V vs. SHE). In this study, all potentials are referred to this electrode. Unless otherwise stated, all electrochemical

experiments were performed without agitation, at 300 K and in darkness. When illumination was needed for the experiment, a white 3 W LED lamp (220 lm, T_c = 2700-3500 K) located at the zenith of the substrate and at 8 cm from it was switched on. For the definition of light pulse (LP) used in this work, we will consider 7 seconds of illumination. After deposition, films were rinsed in deionized water and dried with N_2.

Surface characterization was done by means of a Nanoscope Atomic Force Microscope (AFM) with a Si tip, working in tapping mode and operating in air. Images were analyzed with WSxM 5.0 software and Nanoscope 5.31r1 software. Structural characterization of the Bi layers was done by X-Ray Diffraction (XRD) using a Philips X'Pert PRO system equipped with a Cu target ($\lambda_{K\alpha}$ = 1.54 nm) and a four-circle goniometer. All films were measured in a symmetric Bragg-Brentano configuration ($\theta-2\theta$ scan) to determine the preferred orientation of the films. To avoid substrate reflections, an offset of 0.5º was introduced between the incidence and the diffracted direction ($\omega = \theta - \theta_{offset}$). The crystallographic uniformity of the Bi layers has been analyzed by means of ω–rocking curves (out-of-plane uniformity) and ϕ-scans (in-plane uniformity). The average tilt and twist of Bi grains with respect the GaAs substrate is defined as one half of full width at half maximum (FWHM/2) of ω-rocking curves and ϕ-scans, respectively. In order to extract the FWHM values with their corresponding errors, the ω-rocking curves have been fitted to a pseudovoigt function and the ϕ-scans to a Gaussian function. The values obtained for the FWHM have been corroborated with the software X'Pert Data Viewer provided by PANalytical B. V.

Finally, the Bi/GaAs interface was characterized electrically by means of current-voltage (*I-V*) curves and capacitance - voltage (*C-V*). Several diodes with 200 μm and 230 μm of diameter were fabricated in the Bi films by standard optical lithography followed by photochemical etching. Afterward, an electrical contact made by 20 nm Cr/300 nm Au was evaporated on the top of the Bi diodes to protect them. *I-V* and *C-V* measurements were

carried out at 290 K in a Janis probe station (model CCR10-1) with a Hewlett Packard 4145 semiconductor parameter analyzer and a 4284A LCR meter, respectively. All diodes showed a good reproducibility when measuring the curves, making possible to consider just one *j-V* and *C-V* curve per diode. At least 10 diodes have been measured in each case.

3. Results and Discussion

3.1. Light pulse. Electrodeposition of Bi thin films

The effect of light on the Semiconductor-Electrolyte Interface (ScEI) can be initially detected as a modification of the open circuit potential (OCP) when the n-GaAs electrode is immersed in the Bi(III) solution (Figure 1a). In darkness, the $OCP_{dark} \approx 70$ mV indicates that the GaAs surface is covered by a H_{ads} layer. [10, 12] When the light is switched on, the OCP shifts cathodically, reaching a value of $OCP_{light} \approx -280$ mV, in agreement with previous work [18]. After 7 s, which is denoted as LP as abovementioned, the illumination is switched off and the OCP acquires a value of $OCP_{LP} \approx 40$ mV. The difference between OCP_{dark} and OCP_{LP} indicates that the ScEI has been modified by the LP. However, the difference between OCP_{LP} and the OCP obtained in a H_{ads}-free n-GaAs surface in darkness conditions ($OCP_{free} \approx 100$ mV) [8, 10] reflects that the LP cannot completely remove the H_{ads} layer.

In order to gain further insight into the effect of the LP on the electrochemical properties of the n-GaAs substrate we have performed two CVs (Figure 1b): a) in darkness conditions (denoted as dark), and b) in darkness after applying the LP. The CVs start at the OCP, go first toward the cathodic stage, then to the anodic stage, and finish at the OCP. We can observe that the two CVs, dark and LP, are quite similar. Both curves show a cathodic peak, related to Bi(III) ion reduction, but none exhibit anodic peaks, i.e., the metallic Bi cannot be oxidized into Bi(III) ions during the anodic stage. This is a consequence of the doping level of the n-GaAs substrate, which is low enough to produce a wide space charge region that avoids the necessary electrons tunneling from the electrolyte to the substrate for

the anodic reaction. [12] The onset potential of the Bi(III) ion reduction (defined as the intersection of the rising current of the cathodic peak with its baseline) is E_{onset} *(Bi)* ≈ -230 mV in both cases, which is approximately the onset potential of H^+ reduction. This is a consequence of the presence of the H_{ads} layer on the n-GaAs surface which blocks surface sites that are required for the reduction of Bi(III) ions. [13, 10, 12] When H^+ reduction is activated, some surface sites become free, and Bi (III) ions can get reduced on the n-GaAs surface. Consequently, in H_{ads}-covered n-GaAs substrates, Bi(III) ion reduction takes place simultaneously to H^+ reduction. The similar E_{onset} *(Bi)* obtained for both CVs is a further support to the conclusion that the n-GaAs surface is still covered by H_{ads} after the LP. Although the CV's look similar, if we represent the trace of the cathodic stage in a Tafel plot (inset Figure 1b) we can observe a different slope at low cathodic potentials which indicates a modification of the ScEI as a result of the LP, in agreement with the difference between OCP_{dark} and OCP_{LP} (Figure 1a). Since the n-GaAs surface is still H_{ads} covered, this modification can be a sign of n-GaAs surface degradation produced by light-induced oxidation. [14, 17, 16]

We have electrodeposited 40 nm Bi films in darkness after applying the LP, which have been compared with layers deposited also in darkness but without the previous LP. We have chosen a growth potential of E = -0.3 V (equivalent to an overpotential of $\eta_{SEI} = E - OCP$ = *-0.37 V* [8]) because it is near the region in which a clearer difference between CVs for LP and darkness is observed (Figure 1b). We have analyzed the current density transients obtained during the nucleation of the films (Figure 2a) taking into account the procedure used by other authors [23, 24, 25, 26, 27, 28] that allows the deconvolution of the experimental current density, *j(t)*, into its individual contributions, j_i (with i = *ScEI, des, ads, PR* and *3D*), each one assigned to a different process. This procedure consists in a nonlinear fit of the experimental *j(t)* to a theoretical nucleation model, using the Marquardt−Levenberg algorithm. For cathodic

reactions, where the current density is negative, the absolute value of *j(t)* should be used. In a previous work, we elaborated a theoretical nucleation model based on several processes that occur in the ScEI when it is biased, and that accurately describes the experimental nucleation curves for the electrodeposition of Bi on n-GaAs substrates: [8]

[a] Charging of the ScEI capacitance considering it as a series RC circuit: [29]

$$j_{ScEI}(t) = \frac{Q_{ScEI}}{\tau_{ScEI}} \cdot exp\left(-\frac{t}{\tau_{ScEI}}\right) \quad (1)$$

[b] Desorption of OH^- and ClO_4^- anions:

$$j_{des}(t) = \frac{Q_{des}}{\tau_{des}} \cdot \exp\left(-\frac{t}{\tau_{des}}\right) \quad (2)$$

[c] Adsorption of H^+ via surface states:

$$j_{\mathrm{ads}}(t) = \frac{Q_{ads}}{\tau_{ads}} \cdot \exp\left(-\frac{t}{\tau_{\mathrm{ads}}}\right) \quad (3)$$

The parameters Q_{ScEI}, Q_{des} and Q_{ads} represent the electrical charge involved in each process, and τ_{ScEI}, τ_{des} and τ_{ads} represent their time constants. [25]

[d] Reduction of H^+ on the GaAs surface:

$$j_{\mathrm{PR}} = z_{\mathrm{PR}} \cdot \mathrm{F} \cdot k_{\mathrm{PR}} \quad (4)$$

where z_{PR} is the number of electrons involved in the reduction reaction; F is Faraday's constant; and k_{PR} is the rate constant of the reaction. [30] This expression takes into account the two steps involved in the hydrogen evolution reaction, which follows the Volmer-Heyrovsky route on GaAs substrates in acidic aqueous solutions. [31]

[e] Reduction of Bi(III) ions into metallic Bi following a 3D nucleation controlled by diffusion, and delayed by an induction time, t_0, associated with the initial current decay. [32] This process can be described by the following expression:

$$j_{\mathrm{3D}}(\mathrm{t}) = P_4 \cdot (t - t_0)^{-1/2} \cdot \theta(t - t_0) \quad (5)$$

where $\theta(t)$ is the substrate surface area covered by the diffusion zones of the Bi nuclei. [33]

$$\theta(t) = 1 - exp\left\{ - P_2 \cdot \left[(t - t_0) - \frac{(1 - exp[\,-A \cdot (t - t_0)])}{A} \right] \right\} \quad (6)$$

and

$$P_2 = N_0 \cdot \pi \cdot D \cdot \left(\frac{8\pi \cdot c_0 \cdot M}{\rho} \right)^{1/2} \quad (7)$$

$$P_4 = \left(\frac{z \cdot F \cdot D^{1/2} \cdot c_0}{\pi^{1/2}} \right) \quad (8)$$

where *A, D* and c_o are the nucleation frequency per active site, the diffusion coefficient, and the concentration in the bulk of the electrolyte of Bi(III) ions, respectively; *M* and ρ are the molar mass and the density of metallic Bi; and N_o is the number density of nucleation sites on the GaAs surface.

The nucleation process is divided into two regimes delimited by the induction time, t_0. [8] During the first regime, the ScEI is rearranged due to the modification of the potential from the OCP to the growth potential. During the second regime, the Bi(III) ion reduction (j_{3D}) begins and alters the H^+ reduction (j_{PR}) since the two reactions occur via conduction band states. [34, 31] However, H^+ adsorption (j_{ads}) can run in parallel to Bi(III) ion reduction because they take place at different surface sites and through different electronic states. [35, 25] Therefore, our nucleation model is described by the following equations:

$$j(t) = j_{ScEI}(t) + j_{des}(t) + j_{ads}(t) + j_{PR} \qquad t < t_0 \quad (9)$$

$$j(t) = j_{ads}(t) + j_{PR} \cdot [1 - \theta(t)] + j_{3D}(t) \qquad t > t_0 \quad (10)$$

In order to obtain accurate and reliable results, the experimental current density transients shown in Figure 2a have been fitted to eq. 9 and 10 computing the value, the standard error, and the lower (LCL) and upper (UCL) 95% confidence limits of the parameters Q_{ScEI}, τ_{ScEI}, Q_{des}, τ_{des}, t_0, Q_{ads}, τ_{ads}, k_{PR}, *D*, *A*, and N_0. Table 1 contains the best-fit parameters with their respective errors obtained on basis of the 95% confidence limits being achieved fittings with relative errors below 3 %. In order to extract reliable conclusions, additional transients have been fitted. The average values obtained in each case (dark and LP) exhibit a similar

behaviour than the transients presented in Figure 2a. Deviations up to the 37 % were obtained for some of the parameters due to the sensitivity of this analysis since inhomogeneities of the substrate surface and of the electrodeposited Bi limit the validity of the expressions shown in eq. 1-5, which are derived for ideal both substrates and layers [36].

η_{ScEI} (V)	Dark	LP
τ_{des} (ms)	(7.12 ± 0.10)	(6.57 ± 0.15)
Q_{des} (μC·cm^{-2})	(3.579 ± 0.062)	(1.570 ± 0.044)
t_0 (ms)	(315.5 ± 1.8)	(388.4 ± 1.4)
τ_{ads} (ms)	(60.98 ± 0.52)	(58.71 ± 0.58)
Q_{ads} (μC·cm^{-2})	(27.09 ± 0.12)	(15.606 ± 0.081)
k_{PR} ($\cdot 10^{-10}$ mol·cm^{-2}·s^{-1})	(19.066 ± 0.025)	(14.338 ± 0.014)
D ($\cdot 10^{-8}$ cm^2·s^{-1})	(1205.22 ± 0.41)	(1320.79 ± 0.29)
A (s^{-1})	(2.226 ± 0.015)	(1.6127 ± 0.0075)
N_o ($\cdot 10^5$ cm^{-2})	(5.722 ± 0.016)	(4.5930 ± 0.0087)

Table 1. Best-Fit Parameters and Their Errors Obtained from the Analysis of the Experimental Current Density Transients Shown in Figure 2a.

Figure 2.b and c show that the nucleation model accurately describes the experimental transients, similarly to our previous work. [8, 12] In both cases the charging of the ScEI (j_{ScEI}, red dashed line) is undetectable for the growth potential and time step used. [8, 12] The anion desorption (j_{des}, blue dashed line) has a similar time constant (τ_{des}) in both cases, i.e., the kinetics of this process is not altered by the LP. However, the charge involved in the process (Q_{des}) is smaller in the LP case because some of the anions have already been desorbed during the illumination of the ScEI, when the OCP moves from OCP_{dark} ≈ 70 mV to OCP_{light} ≈ -280 mV. The time constant of the H^+ adsorption process (τ_{ads}) is also similar in both cases, and higher than τ_{des} as expected from previous works. [8, 12] In addition, $\tau_{ads} < t0$, in agreement with previous results obtained for low growth potentials. [12] In the dark case, Q_{ads} is lower than the charge associated with the formation of one monolayer of H_{ads}, q_m = 232 μC cm^{-2},

indicating that the n-GaAs surface is covered by H_{ads} before the electrodeposition [8], in agreement with the value of OCP_{dark} (Figure 1a). Therefore, the small H^+ adsorption that takes place is at the sites that become free after anion desorption (j_{des}). [12] In the LP case, Q_{ads} is also lower than q_m, indicating that the surface is still covered by H_{ads}, in agreement with the conclusions extracted for the values of the OCP (Figure 1a) and $E_{onset}(Bi)$ (Figure 1b). In fact, Q_{ads} is smaller in the LP case than in the dark case, i.e., there are less free surface sites available for the adsorption of H^+ in the LP case. Since H^+ gets adsorbed on surface As atoms, [15] this could indicate that some of them have been removed or chemically altered during the illumination, leaving Ga atoms or other intermediates at the surface where H^+ do not get adsorbed. This further supports the idea of surface degradation during n-GaAs illumination. Although τ_{des} and τ_{ads} are similar in both cases, i.e., the rearrangement of the ScEI takes a similar time in both cases, t_0 is higher in the LP case indicating an inhibition on the start of Bi(III) ion reduction. Finally, k_{PR}, A and N_o are smaller in the LP case, although D is similar in both cases. This indicates that both H^+ and Bi(III) ion reduction are inhibited in the LP case. The values obtained for k_{PR} are similar to our previous work [12], and similar to those obtained by Palomar-Pardavé *et al.* [30] for H^+ reduction on the surface of cobalt nuclei at low overpotentials.

Once the transients have been deconvoluted, it is possible to represent the j_{3D} contribution in a dimensionless plot according to the theoretical model derived by Scharifker and Hills [37] (Figure 2d). The nucleation of the Bi films is clearly mixed in darkness and after illumination. This results from the low values of both N_0 and A (Table 1). The small N_0 is a consequence of the n-GaAs surface blockade by H_{ads} since it restricts the reduction of Bi(III) ions to those surface sites that become free of H_{ads} after H^+ have been reduced on them. The low A responds to the low Bi growth overpotential ($\eta_{Bi} = E - E_{onset}(Bi)$) [19].

Therefore, despite N_0 being small, the low A factor makes not possible to achieve N_0 quickly enough, and a mixed nucleation is reached. [38]

To sum up, on the basis of the OCP values, the CV curves and the analysis of the current density transients, we can conclude that illuminating the n-GaAs surface for a few seconds under open-circuit conditions does not remove the H_{ads} layer. On the contrary, it produces a modification of the n-GaAs surface that has an inhibitory effect on the reduction of Bi(III) ions and H^+, as well as on H^+ adsorption, but it does not affect the type of nucleation (mixed).

3.2. From light pulse to continuous illumination. n-GaAs surface degradation

To confirm that the n-GaAs surface is degraded by light-induced oxidation reactions [18, 39, 14, 16, 17], we have analyzed by AFM the n-GaAs surface as a function of the time of light exposure while immersed in the Bi(III) solution (Figure 3.a-e). The depth profiles show a progressive degradation of the substrate surface with the time of light exposure, confirmed by the continuous increase of the root mean square (rms) roughness and the peak-to-peak (PP) values (Figure 3f). According to Li and Peter [17], the surface degradation is a result of lattice decomposition due to the following photo-oxidation reactions involving photogenerated holes:

$$GaAs + 3H_2O + 3h^+ \rightarrow GaO_3^{3-} + As + 6H^+ \qquad (E_0 = 0.256 \text{ V vs Ag/AgCl}) \qquad (11)$$

$$GaAs + 5H_2O + 6h^+ \rightarrow GaO_3^{3-} + AsO_2^- + 10H^+ \qquad (E_0 = 0.180 \text{ V vs Ag/AgCl}) \qquad (12)$$

The photogenerated holes are deviated to the n-GaAs surface where they break surface As-Ga bonds, altering the surface chemical composition and leading to lattice decomposition. In order to maintain the electrical neutrality of the cell under OCP (zero-current) conditions, reactions involving electrons must be established. In n-GaAs photo-corrosion, this reaction is usually H^+ reduction [17, 16]. However, taking into account the experimental value of

OCP_{light} obtained in this work, we can expect that Bi(III) ions reduction is also involved in the electrons reaction, leading to electroless deposition of Bi. In fact, Vereecken and Searson have already observed the electroless deposition of Bi on n-GaAs(100) substrates under illumination [34].

3.3. Continuous illumination. Electroless deposition of Bi flakes

The illumination of the n-GaAs substrate immersed into the Bi(III) solution produces the degradation of its surface but also the electroless deposition of Bi, as abovementioned. Considering that these two phenomena occur simultaneously, we have explored the possibility of combining them to electrochemically produce Bi flakes. For that, we have continuously illuminated the n-GaAs substrate after being immersed in the electrolyte. In figure 4 we present the OCP evolution with time during the electroless growth of Bi flakes. The curve is spiky and the average value slightly increases during the illumination. After 30 s, Bi islands can be seen naked-eye, and after 5 minutes the n-GaAs surface is covered by unconnected Bi flakes (Figure 5a and b). The electroless process is similar to an electrodeposition growth, with three simultaneous crystal-building mechanisms: nucleation, growth and coalescence of the nuclei to form a thin film. [19] However, some regions of the n-GaAs surface remain free of any deposit independently of the duration of the illumination, corroborating the inhibitory effect of light on the Bi(III) ions reduction deduced from the current density transients (Table 1). The discontinuity of the electroless deposited Bi film has also been observed by Vereecken and Searson. [34] The thickness of the Bi flakes after 5 minutes of illumination as measured by AFM is around 100 nm (Figure 5c).

The simultaneity of Bi electroless deposition and n-GaAs degradation can be explained on basis of the modifications experimented by the energy band diagram of the ScEI when applying light (Figure 6). The n-GaAs/Bi(III) electrolyte junction can be treated as a Schottky barrier where Bi(III) solution plays the role of the metal and the surface states of the n-GaAs

behave like the interfacial states of the Schottky barrier. [8, 12] In darkness, the position of the conduction band (CB) and the valence band (VB) edges at the surface can be extracted from literature [12]: $E_{C,s}$ = -3.74 eV, and $E_{V,s}$ = -5.16 eV (Figure 6a). The position of the Fermi level (E_F) at the ScEI in equilibrium is given by OCP_{dark} ≈ 70 mV, which is -4.77 eV translated to the energy scale. [39] This position approximately coincides with that obtained by photocapacitance spectroscopy for the highest occupied level of surface states associated with surface unsaturated bonds ($E_1 = E_{C,s} - 0.98$ eV). [40] This indicates that surface dangling bonds (SS_{int}) are filled, i.e., saturated by adsorbed species, being the reason for the absence of surface reconstructions in liquid media [41]. Depending on the type of ion adsorbed at the surface, the OCP can slightly vary from 70 mV (adsorbed protons) to 100 mV (adsorbed anions) due to the different effect that each type of ion produces on the surface dipole. [10] From the carrier concentration in the bulk (n_0), we can extract the position of E_F with respect to the edge of the CB in the bulk (E_C) according to Maxwell-Boltzmann statistics: [42]

$$E_C - E_F = -k_B T \cdot ln\left(\frac{n_0}{N_c}\right) = 58\ meV \tag{13}$$

where N_c (= $4.7 \cdot 10^{17}$ cm^{-3}) is the effective density of states for electrons in the conduction band in GaAs [42].

When the ScEI is illuminated, photons (γ) create electron-hole pairs that are separated by the potential gradient in the ScEI related to the band bending. The photogenerated electrons (Δn) move towards the bulk whereas photogenerated holes (Δp) move towards the surface. [43] This charge migration is equivalent to a forward bias called photopotential (V_{ph}) that moves E_F upwards (Figure 6b). Consequently, the OCP (equivalent to E_F) moves from a positive value (OCP_{dark} ≈ 70 mV, i.e., -4.77 eV) to a negative value (OCP_{light} ≈ -280 mV, i.e., -4.42 eV). The photogenerated carriers increase the electrons and holes densities to above their equilibrium populations (n_0 and p_0). [43, 39] and the Fermi level splits into two quasi Fermi levels, one for electrons (F_N) and one for holes (F_P), where $qV_{ph} = F_N - F_P$. [43] The splitting

of the Fermi level allows simultaneous cathodic and anodic reactions. These reactions involve electrons with redox potentials under F_N, whereas anodic reactions involve holes with redox potentials above F_P. For an n-type semiconductor at low injection conditions as in this work, the photogenerated carriers have little influence on the equilibrium population of the majority carriers ($\Delta n << n_0$), but significantly modify the minority carrier density ($\Delta p >> p_0$). Therefore, F_N remains close to the bulk E_F whereas F_P moves toward the VB. It has been observed by several authors that illumination shifts anodically the flat band potential of n-GaAs electrodes between (0.15 – 0.37) V [17, 35, 15, 39], making $E_{C,S}$ and $E_{V,s}$ more negative (unpinning of the band edges). [39] This shift is a consequence of surface degradation produced by the photogenerated holes [44, 17, 15] which occurs only if F_P lies under the energy levels assigned to the anodic reactions shown in eq. 11 and 12, i.e., under -4.96 eV, (Figure 6b). Moreover, electrons must be transferred to the electrolyte to maintain the electrical neutrality of the cell under the open-circuit conditions. Therefore, since F_N lies above the energy level of Bi(III) ion and H^+ reduction (Figure 6b), the electrons transferred to the electrolyte promote these two reactions without applying any growth potential, i.e., Bi can be grown by electroless deposition.

To sum up, the photo-oxidation of the n-GaAs surface (anodic reaction) and the electroless deposition of Bi together with H^+ reduction (cathodic reactions) can take place simultaneously under illumination at open-circuit conditions due to the splitting of the Fermi level produced by the photogenerated carriers.

3.4. Morphological and structural characterization

Figures 7a - c show AFM images measured on the Bi grown in darkness, in darkness after applying a LP, and by electroless deposition under continuous illumination during 5 minutes, respectively. The characterization of the surface morphology was performed just after the Bi synthesis. In addition, we have observed that ambient oxidation does not

significantly modify the Bi layers surface morphology in several weeks. The film grown completely in darkness is taken as the reference as it represents the state of the art for Bi thin films on lower-doped GaAs substrates. It exhibits a surface with small rounded islands and a rms of (7.3 ± 0.7) nm (Figure 7a), in agreement with our previous work [12]. Some areas have a high depth as a consequence of the H_{ads} layer, which leads to a slightly porous film. [13, 12] The morphology of the layer deposited after the LP is applied is pretty similar (Figure 7b), and the rms is nearly the same, (8.2 ± 1.2) nm. Therefore, the inhibitory effect of the LP on the nucleation process observed in the current density transients only slightly increases the rms. On the contrary, the morphology observed in the Bi flakes obtained by electroless deposition presents more elongated islands and a higher rms, (15.8 ± 0.6) nm (Figure 7c), resembling what is obtained when electrodepositing under a low overpotential, η_{SEI}. [8] This can be explained taking into account that OCP_{light} ≈ -0.28 V is more positive than the potential applied in the dark and LP case (E = -0.3 V). The Bi flakes also present areas with a higher depth than the film thickness.

The XRD patterns exhibit in Figure 8 show that in the three cases it is obtained a (012) texture assigned to the rhombohedral structure of metallic Bi ($R\bar{3}m$, 166) with no traces of oxides or secondary compounds. This shows that the substrate orientation has a stronger effect than the growth conditions on the crystal orientation of the electrochemically deposited Bi. [10, 11, 12] The absence of peaks related to other phases in the electroless case in spite of the degradation observed by AFM (Figure 3.a-e) indicates that the subproducts of the n-GaAs surface photo-oxidation (eq. 11 and 12) might be amorphous or rather soluble in the electrolyte. The crystallographic uniformity was study by performing ω-rocking scans around the Bi(024) Bragg reflection instead of the Bi(012) because the GaAs(111) reflection interferes with the latter, whereas the GaAs(222) reflection does not interfere with the Bi(024). In addition, ϕ-scans were performed around the Bi(110) reflection which is the

strongest asymmetric-Bragg reflection, i.e., reflection that is not related to the layer texture. Although it has a 3-fold symmetry, the azimuthal scans show 12 reflections, which indicates that Bi grains are distributed in four possible orientations with respect to GaAs(111)B planes, as we already reported in previous studies. [11, 10] Table 2 shows the average tilt and twist of the Bi grains with respect to the GaAs substrate, obtained as half the FWHM of the peaks observed in the ω-rocking curves and the ϕ-scans, respectively. We can infer that the Bi grains of the films grown in darkness and after applying a LP have a similar average tilt and average twist with respect to the GaAs surface, i.e., the LP does not produce an appreciable effect in the out-of plane nor in the in-plane crystal quality. The electroless deposited Bi flakes also present a similar in-plane quality, but the average tilt is approximately double of that of the dark and the LP case. Although the out-of-plane crystal quality is enhanced with the growth potential [12, 11], the difference between $OCP_{light} \approx$ -0.28 V (electroless case) and *E= -0.3* V (dark and LP case) seems too small to produce such variations of the average tilt. Therefore, we can conclude that the degradation of the n-GaAs surface occurred during the electroless deposition significantly affects the out-of-plane but does not the in-plane crystal quality.

	Dark	**LP**	**Electroless deposition**
Average tilt (º)	(0.1684 ± 0.0019)	(0.1588 ± 0.0020)	(0.3226 ± 0.0053)
Average twist (º)	(6.35 ± 0.58)	(6.10 ± 0.31)	(6.26 ± 0.52)

Table 2. Average tilt and twist obtained from the ω-rocking and ϕ-scans, respectively, measured in the three studied cases.

3.5. Electrical characterization of the interface

Figure 9a shows the experimental *j-V* curves measured in the three samples of electrodeposited Bi. In all cases, the reverse current density is 7 orders of magnitude lower than the forward current density, indicating a good rectifying behaviour, i.e., there is no

significant electron tunneling through the barrier. Consequently, the *j-V* curves should be analyzed on the basis of Thermionic Emission (TE) theory. [45] The current density that flows through the Schottky barrier is described by:

$$j = A^{**}T^2 \cdot exp\left(-\frac{q\phi_B}{k_BT}\right) \cdot \left[-1 + exp\left(\frac{qV_D}{k_BT}\right)\right] \quad (14)$$

where T is the temperature, k_B is Boltzmann constant, q is the elementary charge and V_D is the potential across the Schottky barrier. The Richardson constant A^* is modified into $A^{**} = f_p \cdot f_q \cdot A^*$ to take into account the probability for an electron reaching the metal without being scattered back (f_p) and the quantum-mechanical transmission (f_q). [45] The agreement between the values of the barrier height obtained from the *j-V* and the *C-V* curves depends on the value adopted for A^{**}. The agreement is excellent if we take the value of $3 \cdot 10^4$ A m^{-2} K^{-2}, which has been experimentally evidenced. [46] It should be noticed that this value is only slightly smaller than the theoretical value of $4.4 \cdot 10^4$ A m^{-2} K^{-2} calculated by Crowley and Sze. [47] The potential across the Schottky barrier, V_D, can be extracted from the applied bias, V, by modeling the system like a Schottky diode in series with a resistor of resistance R. This R represents the effect of the bulk of the semiconductor, the electrical contacts, and the probes used to perform the measurements. Consequently:

$$V_D = (V - j \cdot S \cdot R) \quad (15)$$

where S is the area of the diode. In order to obtain a good fit it is necessary to suppose the existence of interfacial states at the Bi/n-GaAs interface. [45] It is usually considered that these states, with a density D_{SS}, are located at an interfacial layer of thickness *d.* Since the XRD measurements do not show traces of oxides or other compounds, these interfacial states must be related to metal-induced gap states (MIGS) or to interfacial defects that act as charge traps. These can be As_{Ga} antisites [48] or other defects produced by the mismatch between the Bi layer and the GaAs surface (Table 2). Due to the presence of the interfacial states, the barrier height presents a dependence on the applied field, i.e., on the applied bias:

$$\phi_b = \phi_b^0 + \frac{\phi_1}{2} - \left\{\phi_1 \cdot \left(\phi_b^0 + \frac{\phi_1}{4} - V_D - \frac{E_C - E_F}{q} - \frac{k_B T}{q}\right)\right\} \quad (16)$$

where E_c -E_F is obtained with eq. 13. The parameter ϕ_1 is related to the characteristics of the interfacial layer:

$$\phi_1 = \frac{2\alpha^2 qn}{\varepsilon_s} \quad (17)$$

where ε_s is the semiconductor dynamic permittivity, which is 10.89·ε_0 for GaAs [49], being ε_0 the vacuum permittivity. The parameter α is

$$\alpha = \frac{d\varepsilon_s}{\varepsilon_i + qdD_{ss}} \quad (18)$$

where ε_i is the permittivity of the interfacial layer. Since this layer seems to be related to the mismatch between the Bi grains and the GaAs substrate, and not to the formation of a new phase, we have considered $\varepsilon_i = \varepsilon_0$. The parameter ϕ_b^0 is the zero-bias barrier height, which is also related to the interfacial layer through the Bardeen model: [45]

$$q\phi_b^0 = \kappa \cdot q(\phi_m - \chi) + (1 - \kappa) \cdot (E_g - \phi_0) \quad (19)$$

where ϕ_m is the metal work function (4.35 V for Bi) [42], χ is the semiconductor electron affinity (4.07 V for GaAs) [42], E_g is the semiconductor band gap (1.42 eV for GaAs) [42] and ϕ_0 is the neutral energy level for the semiconductor metal-induced gap states (0.5 eV for GaAs). [50, 45, 51] The parameter κ is also related to the characteristics of the interfacial layer: [45]

$$\kappa = \frac{\varepsilon_i}{\varepsilon_i + qdD_{ss}} \quad (20)$$

All *j-V* curves have been analyzed by a nonlinear fit of the experimental data to eq. 14 using the Marquardt–Levenberg algorithm, with *R, d* and D_{SS} as free parameters. The fitting provides the uncertainty of these parameters on basis of the 95% confidence limits. The fitting has been limited from 0.45 V to -0.3 V because at higher bias there are additional effects such as local heating. [52] Table 3 lists the weighted average values of *R, d,* and D_{SS} with their

respective errors for each type of deposited Bi. The errors have been calculated taking into account the errors provided by the weighted average and the standard deviation. From *d* and D_{SS}, the zero-bias barrier height, ϕ_b^0, has been obtained according to eq. 19 and eq. 20 and its error has been calculated by propagation of uncertainties. [53] The values collected in Table 3 are accurate, with relative errors lower than 7%, except for *R,* which has a relative error around 15%. We can observed that the films grown in darkness and after applying a LP present the same value of $\phi_b^0(j-V)$, in spite of slightly differences in the values of *d* and D_{ss}. However, the electroless deposited Bi flakes exhibit a lower value of $\phi_b^0(j-V)$.

	Dark	**LP**	**Electroless deposition** (A^{**} = 3·10⁴ A m⁻² K⁻²)	**Electroless deposition** (A^{**} = 5·10⁴ A m⁻² K⁻²)
R (Ω)	4.24 ± 0.66	5.47 ± 0.63	6.92 ± 0.91	6.6 ± 1.0
d (nm)	4.28 ± 0.18	4.55 ± 0.15	4.15 ± 0.15	5.03 ± 0.13
D_{SS} ($\cdot 10^{16}$ eV^{-1} m^{-2})	6.24 ± 0.20	5.835± 0.092	5.82 ± 0.14	5.72 ± 0.13
$\phi_b^0(j-V)$ (V)	0.8103 ± 0.0055	0.8096 ± 0.0040	0.8009 ± 0.0049	0.8168 ± 0.0034
$\phi_b^0(C-V)$ (V)	0.8095 ± 0.0028	0.8053 ± 0.0033	0.8189 ± 0.0013	0.8189 ± 0.0013

Table 3. Weighted Average Values for Resistance (*R*), Interfacial Layer Width (*d*), Density of Interfacial States (D_{SS}), and Zero-Bias Barrier Height obtained by *j-V* Curves ($\phi_b^0(j-V)$) and *C-V* Curves ($\phi_b^0(C-V)$), with their Respective Uncertainties.

In order to verify the values of the barrier height obtained by the *j-V* curves, we have also performed *C-V* curves on each diode since this method gives essentially the value of ϕ_b^0. [45] Figure 9b shows the plot of $(A/C)^2$ vs. *V* derived from the experimental *C-V* curves measured on each case at 290 K and in darkness. The negative values of *V* indicate that the diodes are measured under reverse bias (V_r = -*V*). From the intercept of these curves with the *x*-axis (V_0) we can extract the value of the flat band potential. [45]

$$V_{FB} = V_0 + \frac{k_B T}{q} \tag{21}$$

Then, ϕ_b^0 can be derived as:

$$q\phi_b^0 = qV_{FB} + (E_C - E_F) \tag{22}$$

The values of ϕ_b^0 were weighted averaged for each case to give the values listed in Table 3. We can observe that for the dark and LP films, the interfaces have a similar ϕ_b^0. Moreover, $\phi_b^0(C-V)$ is quite similar to $\phi_b^0(j-V)$, indicating that the model applied in the fitting of the *j-V* curves is adequate. However, for the electroless deposited Bi flakes the value of $\phi_b^0(C-V)$is higher than $\phi_b^0(j-V)$. As we abovementioned, the agreement between *j-V* and *C-V* curves strongly depends on the value of A^{**}, which also depends on f_p and f_q. The quantum-mechanics transmission coefficient (f_q) is closely related to the electrons tunneling mass, m_t. In a previous work, we showed that m_t strongly depends on to the out-of-plane crystal quality. [11] The lower the quality, the lower the m_t, that in turn increases the quantum-mechanical transmission coefficient (f_q), increasing A^{**}. [47] Therefore, since the electroless Bi flakes present a lower out-of-plane structural quality, it is expected a lower m_t, and higher A^{**}. Actually, if we perform the fitting of the *j-V* curve in the electroless deposition case with an $A^{**} = 5 \cdot 10^4$ A m^{-2} K^{-2}, we obtain the same value for $\phi_b^0(j-V)$ and $\phi_b^0(C-V)$ (Table 3). We can observe now that illuminating the substrate decreases the value of D_{ss}, although the time of exposure seems to have little effect on it. This indicates that D_{ss} is sensitive to the chemical composition of the n-GaAs surface beneath the Bi deposit, which is modified by the illumination (eq. 11 and 12) but not by the time of exposure. On the contrary, as the time of exposure to light increases, *d* increases as well (Table 3). This result can be related to the average tilt of the Bi deposits (Table 2). In the dark and LP case, the average tilt is similar as well as the values of *d* (considering the uncertainties). However, in the electroless case, the higher average tilt value is correlated to the higher value of *d*. Therefore, we can

conclude that the value of the Bi/n-GaAs Schottky barrier height is related to both the chemically altered n-GaAs surface and the out-of-plane crystal quality of the interface, in agreement with previous works [11, 12].

4. Conclusions

In this work we have explored the use of light for the electrochemical deposition of Bi on lower-doped n-GaAs(111)B substrates. From the analysis of OCP values, CV curves, and nucleation current density transients, we conclude that a few seconds of illumination at open-circuit conditions does not remove the H_{ads} layer but has an inhibitory effect on the nucleation process due to the photo-oxidation of the n-GaAs surface. However, no significant modifications are detected in the morphological, structural or interfacial electrical properties of a Bi film grown in darkness after this LP. Therefore, the use of light is an unsuccessful approach for improving the quality of Bi films electrodeposited on n-GaAs substrates due to the following reasons: i) if the LP of 7 s does not remove the H_{ads} layer ($Q_{ads} < q_m$; $E_{onset}(Bi,dark) \approx E_{onset}(Bi,LP)$), a shorter pulse would not remove it either; ii) the LP of 7 s produces degradation of the n-GaAs surface, which has a negative effect on the Bi(III) ion reduction; iii) a longer pulse might remove the H_{ads} layer but will also further damage the n-GaAs surface.

The simultaneity of n-GaAs photo-oxidation and Bi electroless deposition at open-circuit conditions allows the synthesis of Bi flakes by means of continuous illumination. When comparing the electroless deposited Bi flakes with Bi layers electrodeposited under dark conditions and after applying the LP, textured Bi(102) with no traces of oxides or alloys is obtained in all cases. The electroless deposition only has a small detrimental effect of the out of plane structural properties. In all cases the interfacial electrical properties are affected by the presence of interfacial states that could be related to the defects caused by the mismatch between the Bi grains and the n-GaAs substrate. The photo-oxidation of the n-GaAs

slightly increases the Schottky barrier height because it both decreases the out-of-plane crystal quality and chemically altered the n-GaAs surface.

Acknowledgement

This work has been financially supported through project MAT2015-66888-C3-3-R of the Spanish Ministry of Economy and Competitiveness (MINECO/FEDER). We would like to acknowledge the postdoctoral fellowship granted by Comunidad de Madrid and the European Union (PEJD-2016/IND-2233). We also acknowledge the use of facilities of Instituto de Sistemas Optoelectrónicos y Microtecnología (ISOM).

REFERENCES

[1] G. E. Smith, G. A. Baraff, J. M. Rowell, Effective g Factor of Electrons and Holes in Bismuth, Phys. Rev. 135 (1964) 1118. DOI: 10.1103/PhysRev.135.A1118.

[2] M. Murata, D. Nakamura, Y. Hasegawa, T. Komine, T. Taguchi, S. Nakamura, C. M. Jaworski, V. Jovovic, J. Heremans, Mean free path limitation of thermoelectric properties of bismuth nanowire, J. Appl. Phys. 105 (2009) 113706. DOI: 10.1063/1.3131842.

[3] G. Smith, Anomalous Skin Effect in Bismuth, Phys. Rev. 115 (1959) 1561. DOI: 10.1103/PhysRev.115.1561.

[4] R. Reneker, New oscillatory absorption of ultrasonic waves in bismuth in a magnetic field, Phys. Rev. Lett. 1 (1958) 440. DOI: 10.1103/PhysRevLett.1.440.

[5] T. Hirahara, K. Miyamoto, I. Matsuda, T. Kadono, A. Kimura, T. Nagao, G. Bihlmayer, E. V. Chulkov, S. Qiao, K. Shimada, H. Namatame, M. Taniguchi, S. Hasegawa, Direct

observation of spin splitting in bismuth surface states, Phys. Rev. B 76 (2007) 153305. DOI: 10.1103/PhysRevB.76.153305.

[6] A. V. Khvalkovskiy, V. Cros, D. Apalkov, V. Nikitin, M. Krounbi, K. A. Zvezdin, A. Anane, J. Grollier, A. Fert, Matching domain wall configuration and spin-orbit torques for efficient domain-wall motion, Phys. Rev. B 87 (2013) 020402(R). DOI: 10.1103/PhysRevB.87.020402.

[7] J. C. Rojas Sánchez, L. Vila, G. Desfonds, S. Gambarelli, J. P. Attane, J. M. De Teresa, C. Magén, A. Fert, Spin-to-charge conversion using Rashba coupling at the interface between non-magnetic materials, Nat. Commun. 4 (2013) 2944. DOI: 10.1038/ncomms3944.

[8] A. Prados y R. Ranchal, Electrodeposition of Bi thin films on n-GaAs(111)B. I. Correlation between the overpotential and the nucleation process, J. Phys.Chem. C 122 (2018) 8874. DOI: 10.1021/acs.jpcc.8b01838.

[9] Z. L. Bao, K. L. Kavanagh, Epitaxial Bi/GaAs diodes via electrodeposition, J. Vac. Sci. Technol. B 24 (2006) 2138. DOI: 10.1116/1.2218874.

[10] A. Prados, L. Pérez, A. Guzmán, R. Ranchal, Mixed effects of the atomic arrangement and surface chemistry on the electrodeposition of Bi thin films on n-GaAs substrates, J. Phys. Chem. C 120 (2016) 28295. DOI: 10.1021/acs.jpcc.6b09144.

[11] A. Prados, R. Ranchal, Electrodeposition of Bi thin films on n-GaAs(111)B. II. Correlation between the nucleation process and the structural and electrical properties, J. Phys. Chem. C 122 (2018) 8886. DOI: 10.1021/acs.jpcc.7b12263.

[12] A. Prados y R. Ranchal, Electrodeposition of Bi films on H covered n-GaAs(111)B substrates, Electrochim. Acta 305 (2019) 212. DOI: 10.1016/j.electacta.2019.03.019.

[13] A. Prados, R. Ranchal, L. Pérez, Blocking effect in the electrodeposition of Bi on n-GaAs in acidic electrolytes, 143 (2014) 23. DOI: 10/1016.j.electacta.2014.07.137.

[14] A. Prados, R. Ranchal, L. Pérez, Strategies to unblock the n-GaAs surface when electrodepositing Bi from acidic solutions, Electrochim. Acta 174 (2015) 264. DOI: 10.1016/j.electacta.2015.05.188.

[15] B. H. Erné, F. Ozanam, J. -N. Chazalviel, The mechanism of hydrogen gas evolution on GaAs cathodes elucidated by in situ snfrared spectroscopy, J. Phys. Chem. B 103 (1999) 2948. DOI: 10.1021/jp984765t.

[16] H. Gerischer, Electrochemical Behaviour of Semiconductors Under Illumination, J. Electrochem. Soc. 113 (1966) 1174. DOI: 10.1149/1.2423779.

[17] J. Li, L. M. Peter, Surface recombination at semiconductor electordes. Part IV., J. Electroanal. Chem. 199 (1986) 1. DOI: 10.1016/0022-0728(86)87038-3.

[18] Y. Huang, J. Luo, D. G. Ivey, Comparative study of GaAs corrosion in H_2SO_4 and NH_3H_2O solutions by electrochemical methods and surface analysis, Mater. Chem. Phys. 93 (2005) 429. DOI: 10.1016/j.matchemphys.2005.03.049.

[19] M. Paunovic y M. Schlesinger, Fundamentals of Electrochemical Deposition, New Jersey: John Wiley & Sons, Inc., 2006

[20] T. Mayer, M. Lebedev, R. Hunger, W. Jaegermann, Elementary processes at semiconductor/electrolyte interfaces: perspectives and limits of electron spectroscopy, Appl. Surf. Sci. 252 (2005) 31. DOI: 10.1016/j.apsusc.2005.01.110.

[21] M. V. Lebedev, T. Masuda, K. Uosaki, Charge transport at the interface of n-GaAs (100) with an aqueous HCl solution: electrochemical impedance spectroscopy study, Semicond. 46 (2012) 471. DOI: .

[22] B. H. Erné, F. Ozanam, J. -N. Chazalviel, Dynamics of hydrogen adsorption on GaAs electrodes, Phys. Rev. Lett. 80 (1998) 4337. DOI: 10.1103/PhysRevLett.80.4337.

[23] M. Palomar-Pardavé, M. Miranda-Hernández, I. González, N. Batina, Detailed characterization of potentiostatic current transients with 2D-2D and 2D-3D nucleation transitions, Surf. Sci. 399 (1998) 80. DOI: 10.1016/S0039-6028(97)00813-3.

[24] F. E. Varela, L. M. Gassa, J. R. Vilche, Kinetics and mechanism of the electroreduction of anodic layers formed on lead in 5 M H_2SO_4 at 25°C, Electrochim. Acta 37 (1992) 1119. DOI: 10.1016/0013-4686(92)85232-a.

[25] M. H. Hölzle, U. Retter, D. M. Kolb, The kinetics of structural changes in Cu adlayers on Au(111), J. Electroanal. Chem. 371 (1994) 101. DOI: 10.1016/0022-0728(93)03235-H.

[26] A. Hernández-Espejel, M. Palomar-Pardavé, R. Cabrera-Sierra, M. Romero-Romo, M. T. Ramírez-Silva, E. M. Arce-Estrada, Kinetics and Mechanism of the Electrochemical Formation of Iron Oxidation Products on Steel Immersed in Sour Acid Media, J. Phys. Chem. B 115 (2011) 1833. DOI: 10.1021/jp106851b.

[27] T. d. J. Licona-Sánchez, G. A. Álvarez-Romero, L. H. Mendoza-Huizar, C. A. Galán-Vidal, M. Palomar-Pardavé, M. Romero-Romo, H. Herrera-Hernández, J. Uruchurtu, J. M. Juárez-García, Nucleation and Growth Kinetics of Electrodeposited Sulfate-Doped Polypyrrole: Determination of the Diffusion Coefficient of SO_4, J. Phys. Chem. B 114 (2010) 9737. DOI: 10.1021/jp102676q.

[28] D. Grujicic, B. Pesic, Electrochemical and AFM study of nickel nucleation mechanisms on vitreous carbon from ammonium sulfate solutions, Electrochim. Acta 52 (2006) 2678. DOI: 10.1016/j.electacta.2005.08.017.

[29] G. Oskam, P. M. Hoffmann, A. Natarajan, P. C. Searson, Semiconductor/electrolyte boundaries, in: J. G. Webster, Wiley Encyclopedia of electrical and electronics engineering, John Wiley and Sons, 2007. DOI: 10.1002/047134608X.W3225.pub2.

[30] M. Palomar-Pardavé, B. Scharifker, E. Arce, M. Romero-Romo, Nucleation and diffusion-controlled growth of electroactive centers. Reduction of protons during cobalt electrodeposition, Electrochim. Acta 50 (2005) 4736. DOI: 10.1016/j.electacta.2005.03.004.

[31] B. H. Erné, M. Stchakovsky, F. Ozanam, J.-N. Chazalviel, Surface composition of n-GaAs cathodes during hydrogen evolution characterized by in situ ultraviolet-visible ellipsometry and in situ infrared spectroscopy, J. Electrochem. Soc. 145 (1998) 447. DOI: 10.1149/1.1838283.

[32] P. M. Rigano, C. Mayer, T. Chierchie, Electrochemical nucleation and growth of copper on polycriystalline palladium, J. Electroanal. Chem. Interfacial Electrochem. 248 (1988) 219. DOI: 10.1016/0022-0728(88)85163-5.

[33] B. R. Scharifker, J. Mostany, M. Palomar-Pardavé, I. González, On the theory of the potentiostatic current transient for diffusion-controlled three-dimensional electrocrystallization processes, J. Electrochem. Soc. 146 (1999) 1005. DOI: 10.1149/1.1391713.

[34] P. M. Vereecken, P. C. Searson, Electrochemical deposition of Bi on GaAs (100), J. Electrochem. Soc. 148 (2001) C733. DOI: 10.1149/1.1406493.

[35] I. Uhlendorf, R. Reineke-Koch, R. Memming, Analysis of the hydrogen formation at GaAs electrodes by impedance spectroscopy investigations, Ber. Bunsenges. Phys. Chem. 99 (1995) 1082. DOI: 10.1002/bbpc.199500038.

[36] J. W. Schultze, D. Dickertmann, Kinetic Investigations of Structural Changes and Desorption of Metal Adsorption Layers on Single Crystal Planes, Faraday Symp. Chem. Soc. 12 (1977) 36. DOI: 10.1039/FS9771200036.

[37] B. Scharifker, G. Hills, Theoretical and experimental studies of multiple nucleation, Electrochim. Acta 28 (1983) 879. DOI: 10.1016/0013-4686(83)85163-9

[38] B. R. Scharifker, J. Mostany, Interfacial Kinetics and Mass Transport, in: A. J. Bard, Bard, M. Stratmann and E. J. Calvo, Encyclopedia of Electrochemistry, Vol. 2, Wiley, New York, 2003, p. 512.

[39] R. Memming, Semiconductor Electrochemistry, Wiley-VCH, Darmstadt, 2001.

[40] P. Allongue, Steady state photocapacitance study of semiconductor/electrolyte junctions II. Surface state distribution and charge transfer mechanisms, Ber. Bunsenges. Phys. Chern. 92 (1988) 895. DOI: 10.1002/bbpc.198800217.

[41] H. Lüth, Surface and interfaces of solid materials, Springer, Berlin, 1995. DOI 10.1007/978-3-662-03132-2.

[42] S. M. Sze, Physics of Semiconductor Devices, John Wiley & Sons, Inc., New York, 1981.

[43] N. Sato, Electrochemistry at metal and semiconductor electrodes, Elsevier Science B.V., Amsterdam, 1998.

[44] P. Allongue, H. Cachet, Band-Edge Shift and Surface Charges at Illuminated n-GaAs/Aqueous Electrolyte Junctions. Surface-State Analysis and Simulation of Their Occupation Rate, J. Electrochem. Soc. 132 (1985) 45. DOI: 10.1149/1.2113788.

[45] E. H. Rhoderick, Metal-semiconductor contacts, IEE Proceedings I - Solid-State and Electron Devices 129 (1982) 1. DOI: 10.1049/ip-i-1.1982.0001.

[46] Y. A. Goldberg, E. A. Posse, B. V. Tsarenkov, Mechanism of flow of direct current in GaAs surface-barrier structures, Sov. Phys. Semicond. 9 (1975) 337.

[47] C. R. Crowell, S. M. Sze, Current transport in metal-semiconductor barriers, Solid-State Electron. 9 (1966) 1035. DOI: 10.1016/0038-1101(66)90127-4.

[48] W. E. Spicer, Z. Liliental-Weber, E. Weber, N. Newman, T. Kendelewicz, R. Cao, C. McCants, P. Mahowald, K. Miyano, I. Lindau, The advanced unified defect model for Schottky barrier formation, J. Vac. Sci. Tec. B 6 (1988) 1245. DOI: 10.1116/1.584244.

[49] V. L. Rideout, C. R. Crowell, Effects of image force and tunneling on current transport in metal-semiconductor (Schottky barrier) contacts, Solid-State Electron. 13 (1970) 993. DOI: 10.1016/0038-1101(70)90097-3.

[50] A. M. Cowley, S. M. Sze, Surface states and barrier height of metal semiconductor Systems, J. Appl. Phys. 36 (1965) 3212. DOI: 10.1063/1.1702952.

[51] W. Mönch, Electronic structure of metal-semiconductor contacts, Springer, Dordrecht, 1990.

[52] R. Stratton, Volt-current characteristics for tunneling through insulating films, J. Phys. Chem. Sol. 23 (1962) 1177. DOI: 10.1016/0022-3697(62)90165-8.

[53] J. R. Taylor, An introduction to error analysis. The study of uncertainties in physical measurements, University Science Books, Sausalito (CA - USA), 1997.

FIGURES CAPTIONS

Figure 1. (a) Evolution with time for darkness and illuminated conditions of the OCP measured on a n-GaAs substrate immersed in the Bi(III) solution. (b) Cyclic voltammetry scans performed on a lower-doped n-GaAs(111)B substrate into the Bi(III) solution in darkness (dark) and after applying a short light pulse (LP). Inset: Tafel plot of the cathodic stage

Figure 2. (a) Current density transients recorded during the nucleation of the Bi films grown at -0.3 V in the dark case and the LP case. Inset: enlargement of the initial decay of the current density. Deconvolution of the current density transient recorded during the nucleation of the Bi film grown (b) under darkness and (c) after applying a LP. Insets: enlargement of the initial current density decay. (d) Non-dimensional plot of the j_{3D} contributions, and theoretical curves for instantaneous and progressive nucleation.

Figure 3. AFM images with their respective depth profile below each image measured on n-GaAs substrates (a) not illuminated, and illuminated for (b) 7 s, (c) 1 min, (d) 2 min and (e) 5 min while being immersed in the Bi(III) solution. (e) Evolution of rms and PP values measured in the AFM images shown in Figure 3.

Figure 4. OCP evolution with time during the electroless growth of Bi flakes.

Figure 5. Optical micrographs of an n-GaAs subtrate covered by electroless deposited Bi flakes obtained with magnification (a) x10 and (b) x100. (c) AFM image and representative depth profiles marked from (1) to (3) obtained in the area marked in (b) with a dark grey square.

Figure 6. Energy band diagram at open-circuit conditions of a ScEI formed by the Bi(III) solution and the n-GaAs substrate (n_0 = 4 × 10^{16} cm^{-3}) (a) in darkness and (b) under

illumination. The energy scale is referred to the vacuum level, whereas the potential scale is referred to the Ag/AgCl reference electrode ($E_{Ag/AgCl}$ = 0.196 V vs SHE).

Figure 7. AFM images and representative depth profiles shown below each image measured on the Bi electrochemically deposited on n-GaAs(111)B substrates at -0.3 V (a) in darkness and (b) after applying a LP, and (c) the Bi flakes grown by electroless deposition.

Figure 8. Bragg−Brentano XRD patterns of the Bi layers deposited on n-GaAs(111)B substrates at -0.3 V in darkness (black line) and after applying a LP (orange line), and the Bi flakes grown by electroless deposition (blue line). The dashed lines indicate the position of Bi reflections (ICDD card 00-044-1246) that matches with an observed peak. Peaks marked with * correspond to GaAs(333) reflections.

Figure 9. (a) Experimental and fitted *j-V* curves. (b) *(C/A)-V* and $(C/A)^{-2}$-*V* curves.

Highlights:

- Bi(III) ion reduction on n-GaAs is inhibited by an adsorbed hydrogen layer (H_{ads}).
- The H_{ads} layer is not removed upon illumination.
- Illumination causes simultaneous Bi(III) ion reduction and n-GaAs oxidation.
- Photo-oxidized n-GaAs hinders Bi(III) ion reduction but promotes Bi flakes.

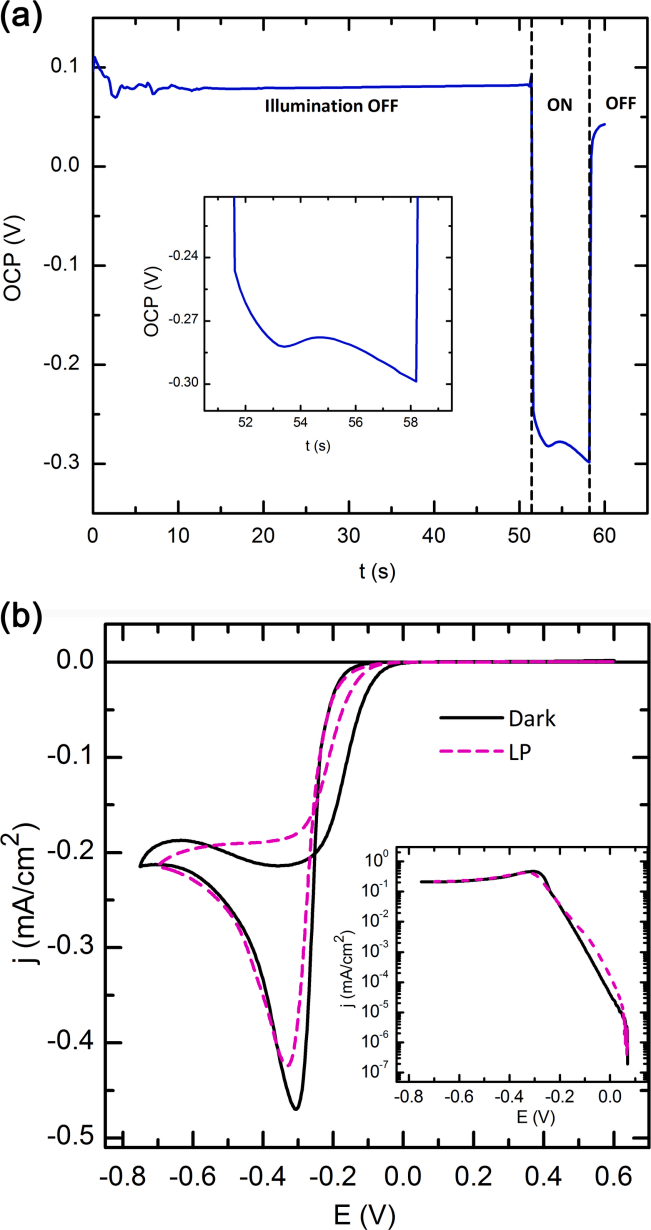
(a)
Illumination OFF
ON
OFF
OCP (V)
t (s)
(b)
Dark
LP
j (mA/cm2)
E (V)

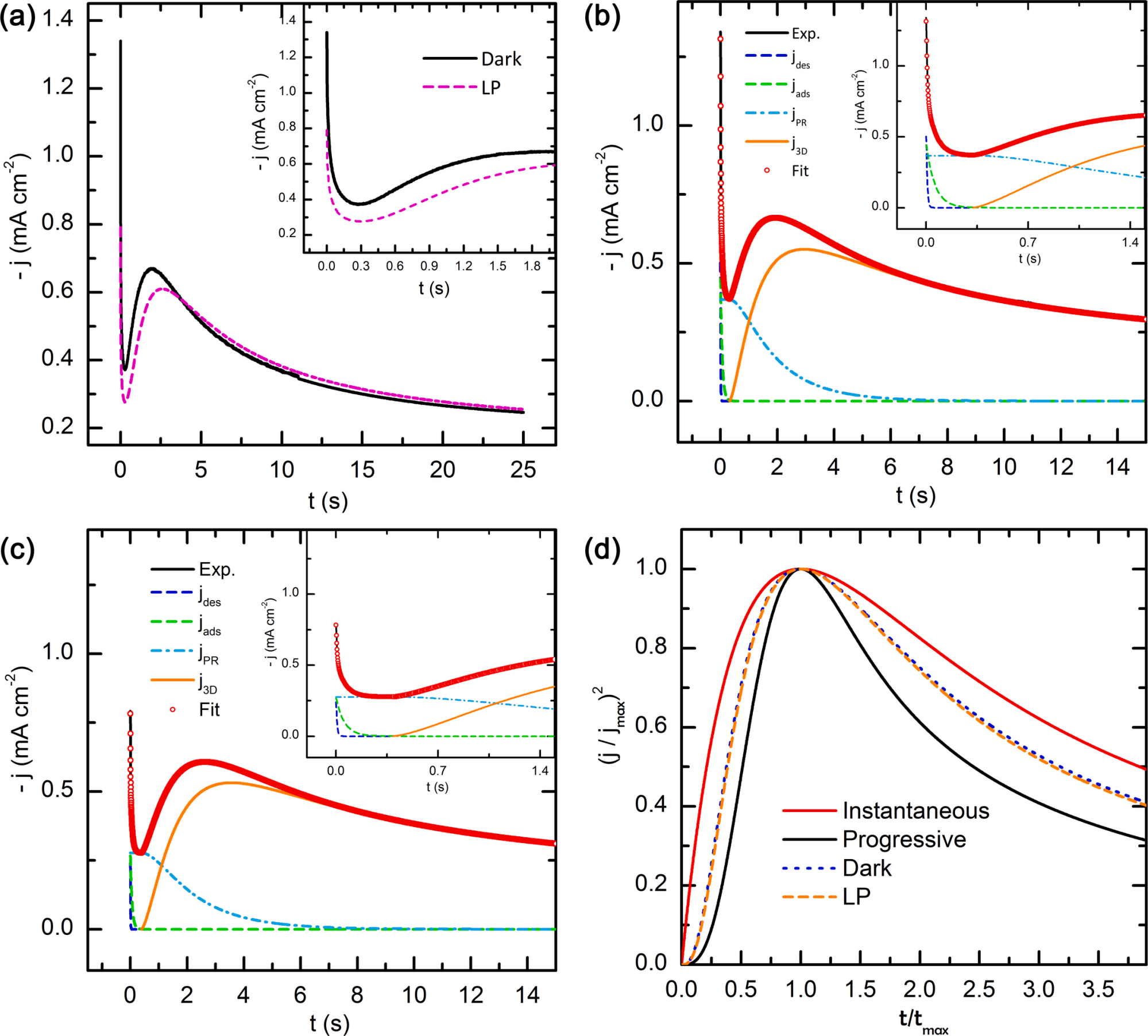
(a)
- j (mA cm-2)
t (s)
Dark
LP
(b)
Exp.
jdes
jads
jPR
j3D
Fit
(c)
(d)
(j / jmax)2
t/tmax
Instantaneous
Progressive
Dark
LP

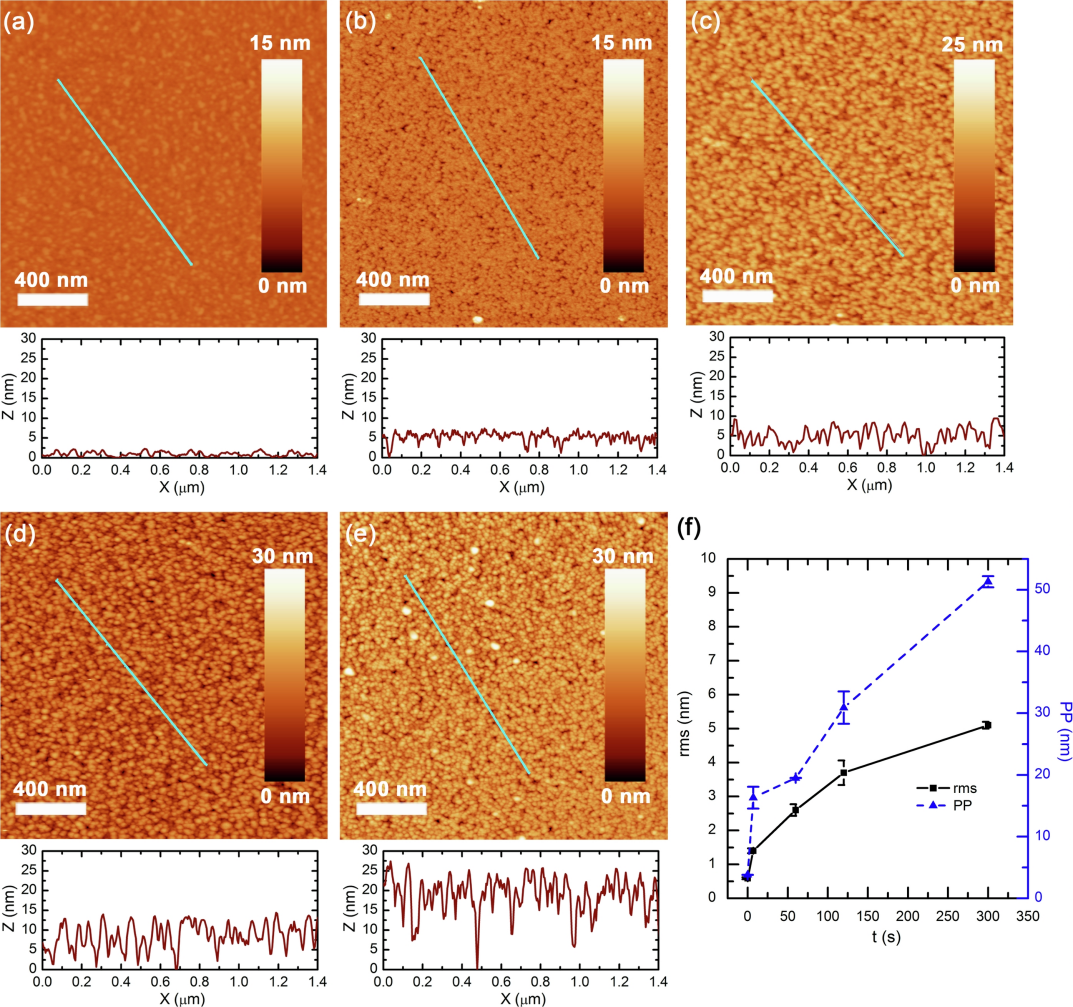
(a)
15 nm
0 nm
400 nm
(b)
15 nm
0 nm
400 nm
(c)
25 nm
0 nm
400 nm
Z (nm)
X (μm)
(d)
30 nm
0 nm
400 nm
(e)
30 nm
0 nm
400 nm
(f)
rms (nm)
PP (nm)
t (s)
rms
PP

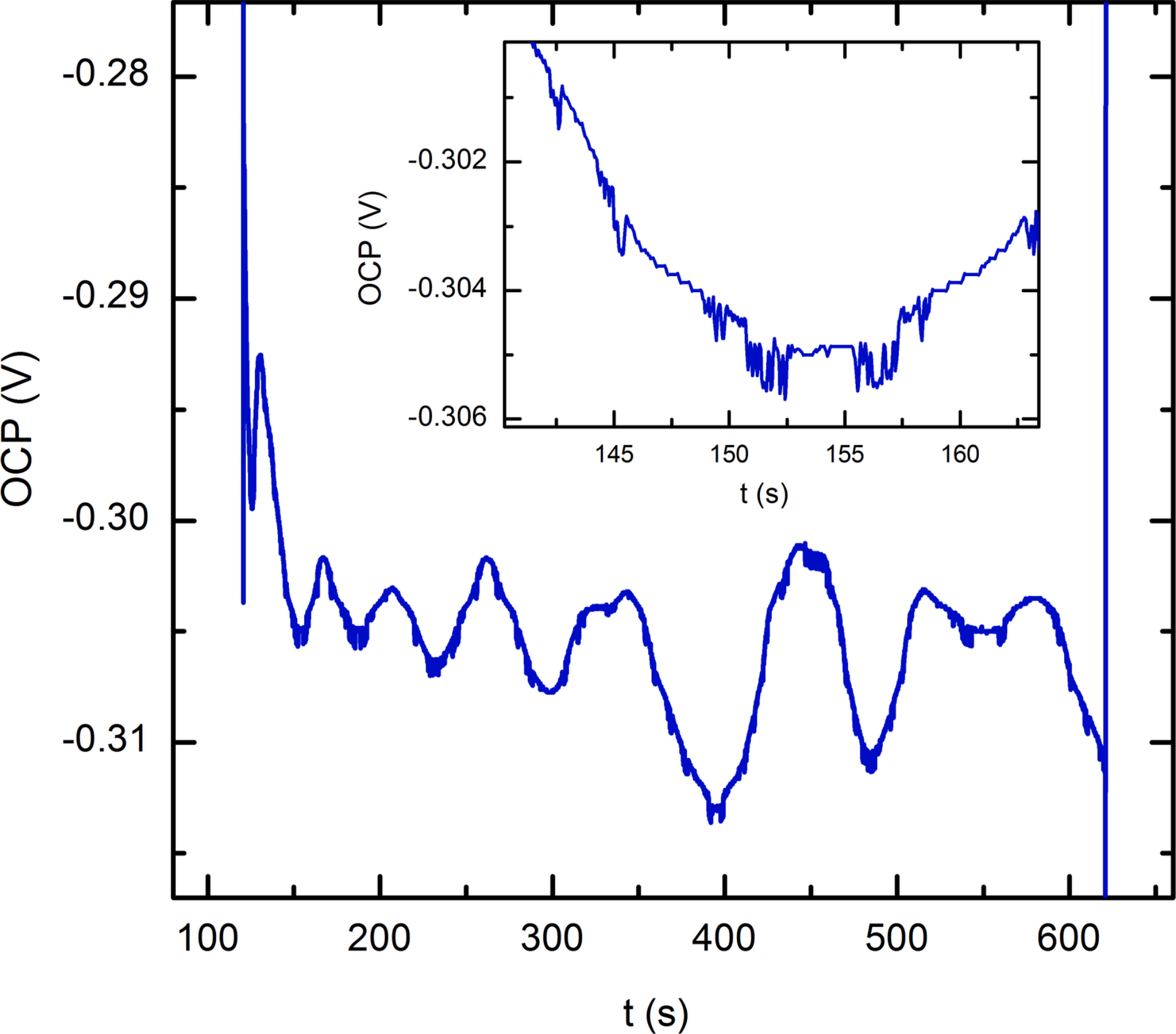
-0.28
-0.29
-0.30
-0.31
OCP (V)
100
200
300
400
500
600
t (s)
-0.302
-0.304
-0.306
OCP (V)
145
150
155
160
t (s)

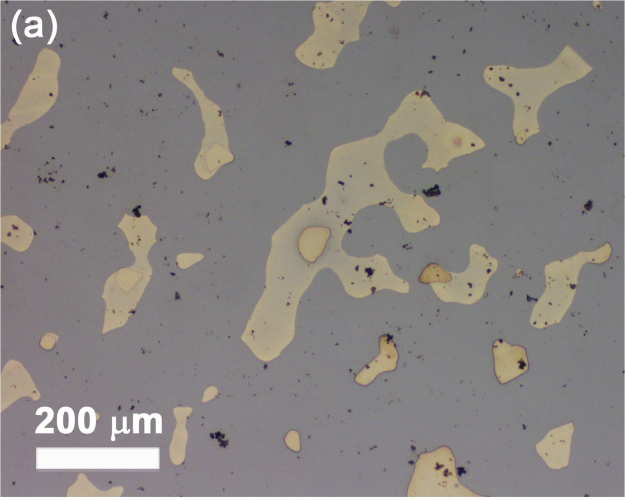
(a)
200 μm

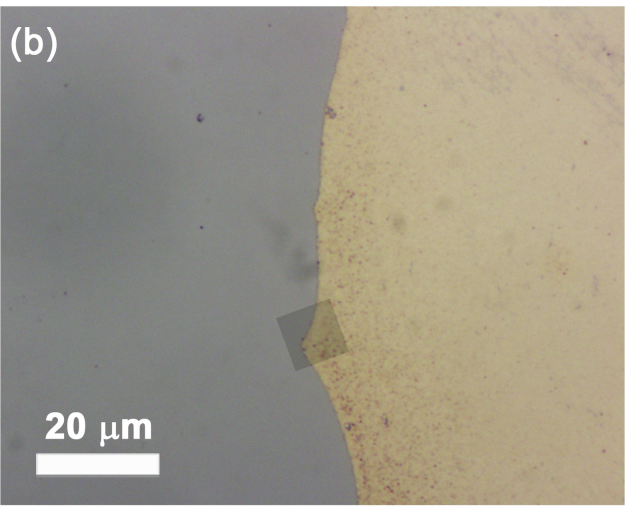
(b)
20 μm

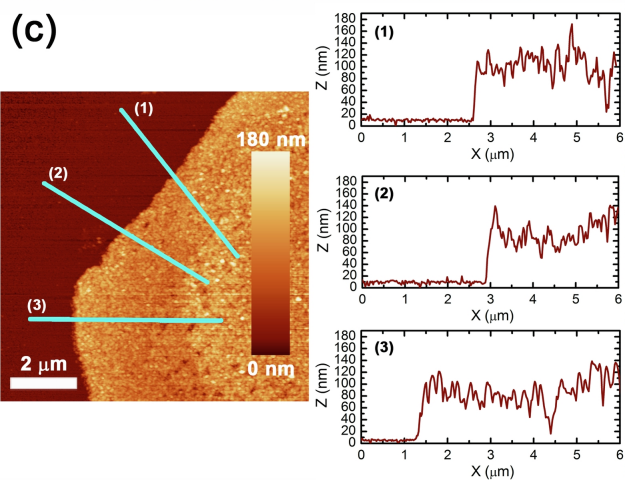
(c)
(1)
(2)
(3)
180 nm
0 nm
2 μm
Z (nm)
X (μm)

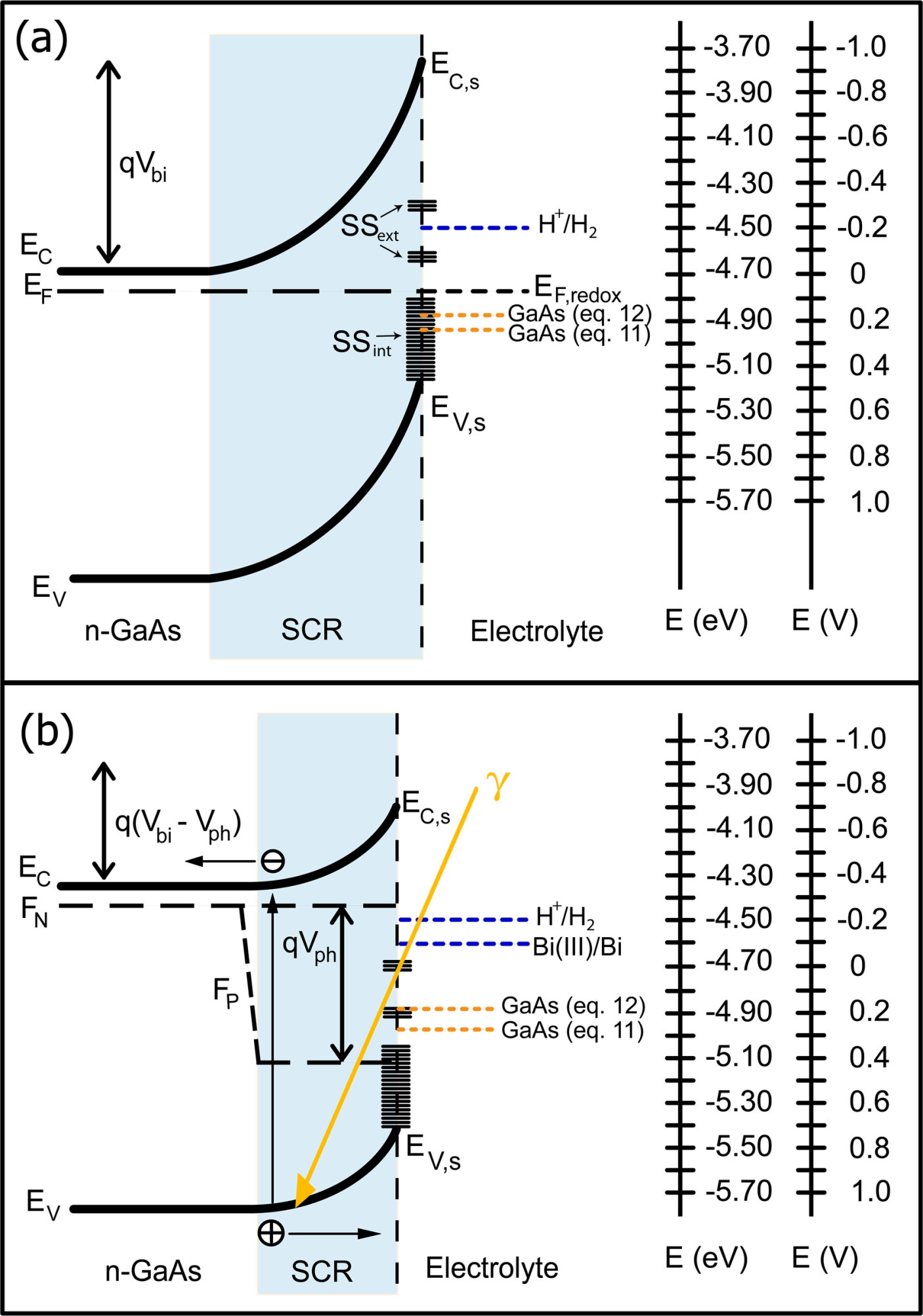
(a)
qV_{bi}
$E_{C,s}$
E_C
E_F
SS_{ext}
H^+/H_2
$E_{F,redox}$
GaAs (eq. 12)
GaAs (eq. 11)
SS_{int}
$E_{V,s}$
E_V
n-GaAs
SCR
Electrolyte
-3.70
-3.90
-4.10
-4.30
-4.50
-4.70
-4.90
-5.10
-5.30
-5.50
-5.70
E (eV)
-1.0
-0.8
-0.6
-0.4
-0.2
0
0.2
0.4
0.6
0.8
1.0
E (V)
(b)
$q(V_{bi} - V_{ph})$
$E_{C,s}$
E_C
F_N
qV_{ph}
F_P
H^+/H_2
Bi(III)/Bi
GaAs (eq. 12)
GaAs (eq. 11)
$E_{V,s}$
E_V
γ
n-GaAs
SCR
Electrolyte
-3.70
-3.90
-4.10
-4.30
-4.50
-4.70
-4.90
-5.10
-5.30
-5.50
-5.70
E (eV)
-1.0
-0.8
-0.6
-0.4
-0.2
0
0.2
0.4
0.6
0.8
1.0
E (V)

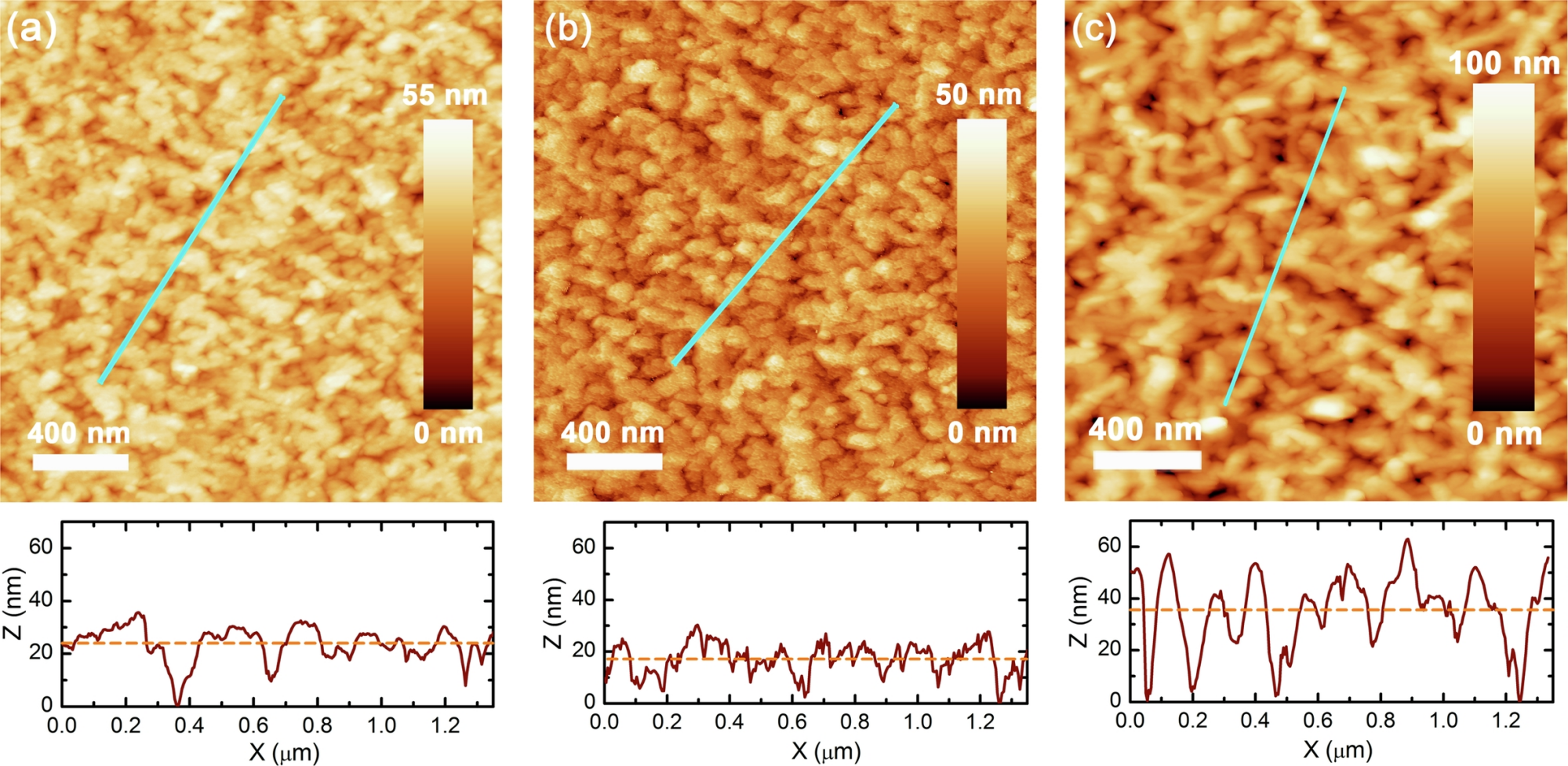
(a)
55 nm
0 nm
400 nm
(b)
50 nm
0 nm
400 nm
(c)
100 nm
0 nm
400 nm
Z (nm)
X (μm)
0
20
40
60
0.0
0.2
0.4
0.6
0.8
1.0
1.2

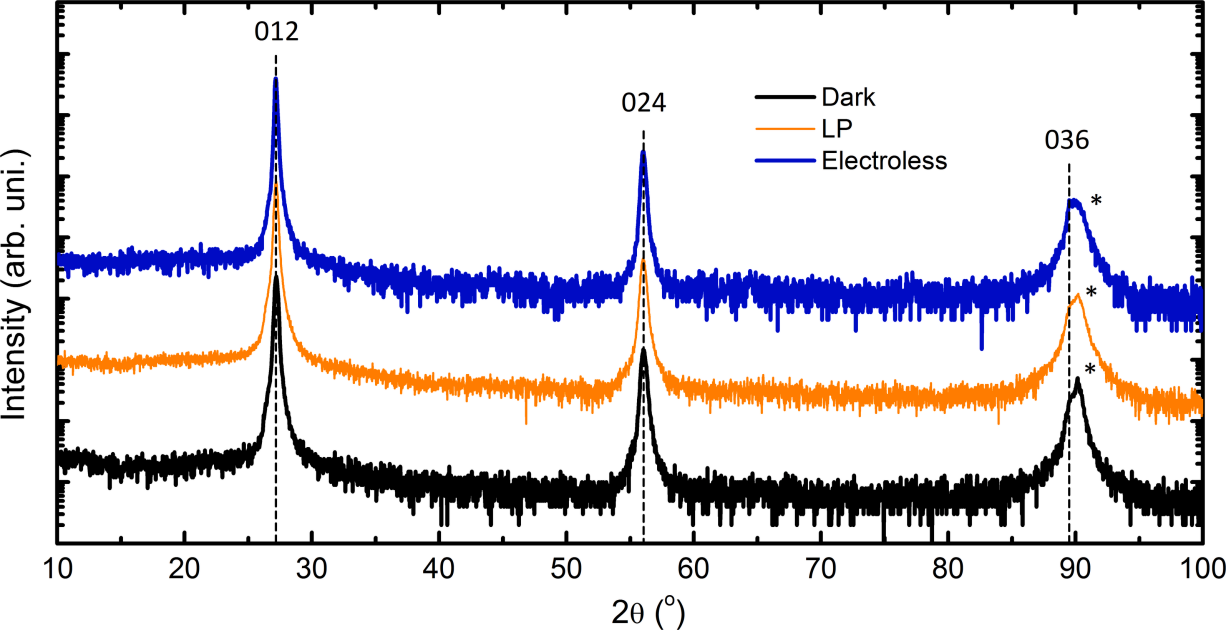
012
024
036
Dark
LP
Electroless
*
*
*
Intensity (arb. uni.)
10
20
30
40
50
60
70
80
90
100
2θ (°)

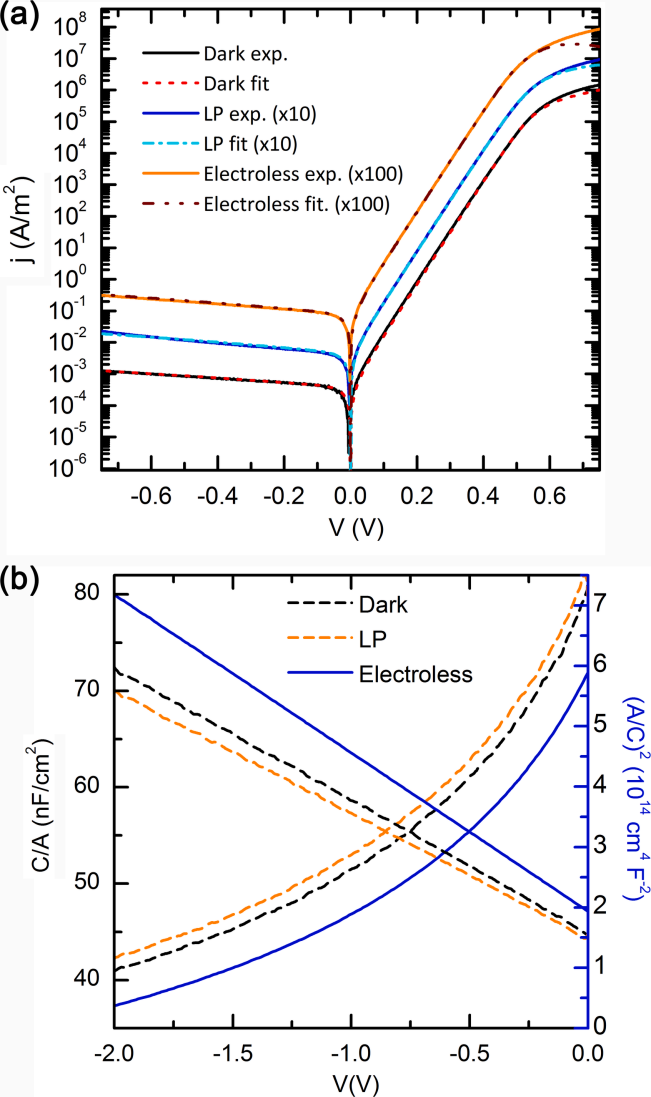
(a)
Dark exp.
Dark fit
LP exp. (x10)
LP fit (x10)
Electroless exp. (x100)
Electroless fit. (x100)
j (A/m^2)
V (V)
(b)
Dark
LP
Electroless
C/A (nF/cm^2)
(A/C)^2 (10^{14} cm^4 F^{-2})
V(V)

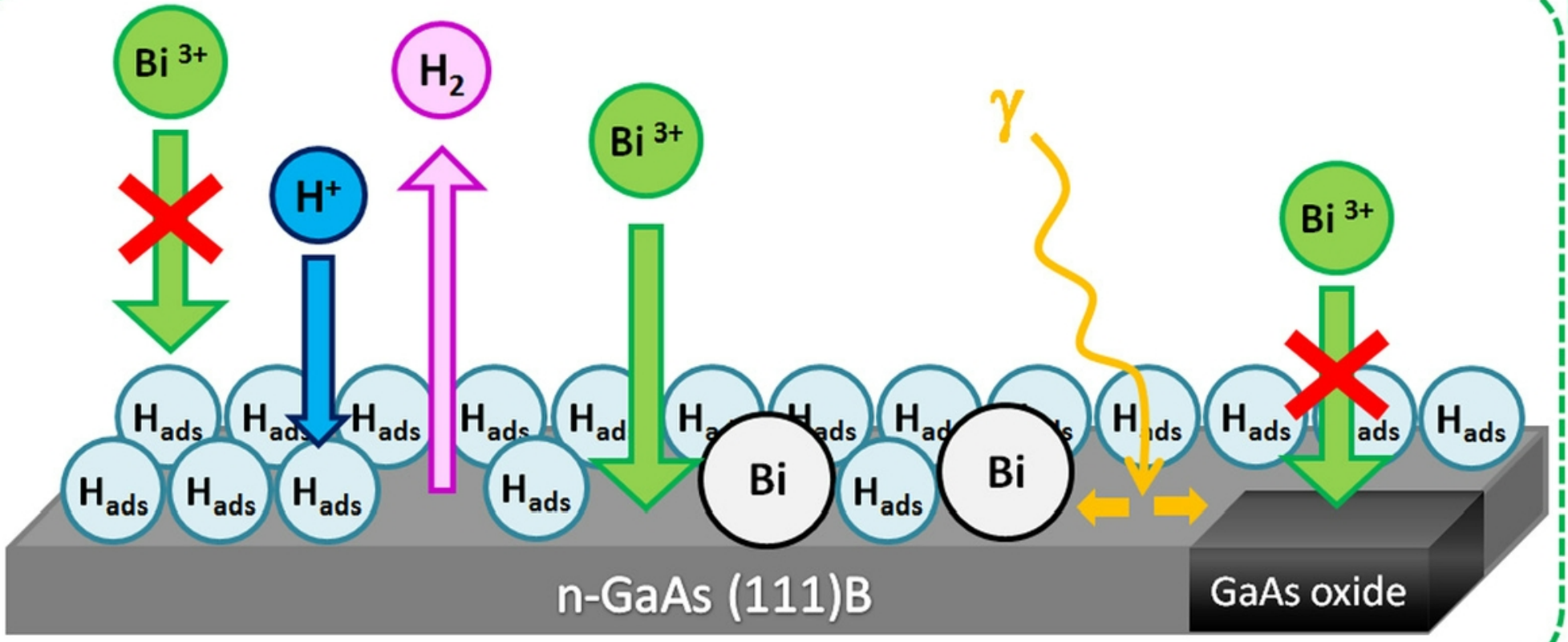
Bi 3+
H2
H+
Bi 3+
γ
Bi 3+
Hads
Bi
Bi
n-GaAs (111)B
GaAs oxide